DES vs RANS: The flatback airfoil case

DES vs RANS: The flatback airfoil case

George Papadakis[1], Marinos Manolesos[2], Konstantinos Diakakis[3] and Vasilis A. Riziotis[3]

[1]School of Naval Architecture & Marine Engineering, National Technical University of Athens, GR15780 Athens, Greece
[2]College of Engineering, Swansea University, Bay Campus, Fabian Way, Swansea, UK, SA1 8EN
[3]School of Mechanical Engineering, National Technical University of Athens, GR15780 Athens, Greece

E-mail: papis@fluid.mech.ntua.gr

Abstract. Using flatback airfoils at the root of wind turbine (WT) blades is becoming more popular as the WTs increase in size. The reason is that they provide significant aerodynamic, aeroelastic and structural benefits. However, due to the blunt trailing edge (TE) , the wake of such airfoils is highly unsteady and rich in three-dimensional vortical structures.This poses significant challenges on the numerical simulation of the flow around them, given the highly unsteady, three-dimensional turbulent character of their wake. In this work, computational predictions for a flatback airfoil employing both RANS and DES approaches on three successively refined grids up to 25 million cells are compared with available experimental data. Results suggest that even though URANS and DDES are in good agreement in terms of lift and drag, RANS simulations fail to accurately capture the turbulent wake unsteady characteristics.

1. Introduction

The practice of incorporating flatback airfoils, i.e. airfoils with a blunt trailing edge (TE), at the root of wind turbine (WT) blades is becoming popular as WT rotor diameters increase in size. The reason is that they offer several aerodynamic, structural and aeroelastic benefits. In regards to aerodynamic performance, flatback airfoils can provide higher lift values due to the reduced adverse pressure gradient over the aft part of the suction side [1]. Moreover, their aerodynamic performance is insensitive to surface roughness when compared to that of traditional sharp trailing edge airfoils [1]. In fact it has been shown that blades with flatback airfoils can be up to 16% lighter than blades that use traditional airfoils without any performance penalty [2]. Additionally, flatback blades have increased flapwise stiffness, due to the blunt TE and increased blade cross-sectional area, which both are beneficial in terms of the structural design. Finally, trailing edge flow control devices can be easily accommodated in order to improve their performance and decrease the associated drag penalty [3, 4].

On the other hand, the blunt trailing edge leads to the formation of a von Karman street-like wake. This inherent pitfall of flatback airfoils requires careful investigation of the shedding frequencies that may lead to vortex-induced vibrations (VIV), as the latter can eventually shorten the WT lifespan.

In regard to numerical analysis, these types of flow problems are often tackled by Unsteady Reynolds-Averaged Navier Stokes (URANS) solvers, which commonly utilize conventional one

and two-equation turbulence models. URANS solvers are not suitable for the simulation of inherently unsteady separated flows, because they underpredict turbulence levels in the wake and tend to artificially restrict flow three-dimensionality, resulting in patterns that closely resemble 2D-like flows [5].

The increased availability of computational resources has, in turn, increased the popularity of higher fidelity turbulence modeling approaches, such as Large Eddy Simulation (LES). However, grid requirements for LES at practical Reynolds numbers ($Re > 10^6$) remain prohibitive. An attractive way to alleviate computational demands for the simulation of separated flows is to utilize hybrid RANS-LES turbulence models like Detached Eddy Simulation (DES), or its variants Delayed DES (DDES) [6] and Improved Delayed DES (IDDES) [7].

In the present work, the flow past a 30% thick airfoil with a 10% thick TE is investigated using both URANS and IDDES approaches on identical grids of varying density. The predictions are compared to previously published wind tunnel results [8]. The considered flow case is at a low Angle of Attack (AoA) and remains attached over the airfoil surface. However, the focus of the present comparison is on the wake downstream of the blunt TE, which is highly unsteady. Results from experiments and numerical simulations are compared in terms of both integrated loads (mean C_L and C_D, Strouhal numbers) and wake behavior (Reynolds Stresses and velocity contours).

2. Experimental and Numerical Setup

2.1. Experimental Setup

The numerical results are compared against Stereo Particle Image Velocimetry (PIV), forces and hot wire measurements in the wake of the airfoil. In the experiments, the chord based Reynolds number was $Re = 1.5 \cdot 10^6$, the model chord $c = 0.5m$ and the model aspect ratio $AR = 2$. Figure 2 presents a schematic of the experimental setup, where the Stereo PIV measurement plane is shown along with the location of the hot wire probe in the wake of the airfoil. Extensive description of the wind tunnel tests can be found in [8].

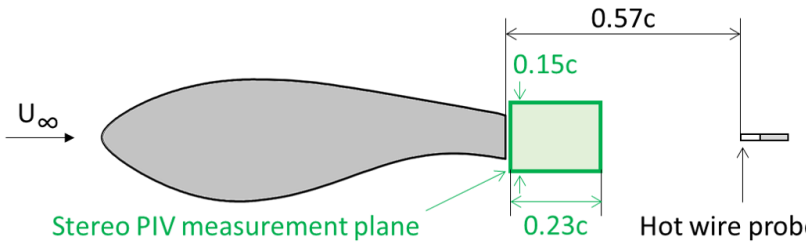

Figure 1: Schematic of the experimental set-up, showing the flatback airfoil under investigation, LI30-FB10, the location of the hot wire probe in the wake and size of the Stereo PIV measurement plane.

2.2. Numerical Framework

The CFD solver used for the numerical simulations is MaPFlow ([9],[10],[11]), which is developed at the Laboratory of Aerodynamics of NTUA. MaPFlow is a compressible, cell-centered solver that can use both structured and unstructured grids. The convective fluxes are discretized using the approximate Riemann solver of Roe [12] with Venkatakrishnan's limiter [13], while the viscous fluxes are discretized using a second order piecewise linear scheme. Simulations of flows in the incompressible region are feasible using Low Mach Preconditioning.

For the URANS simulations presented in this work, the Spalart-Allmaras (SA) one-equation RANS model was used [14]. In regards to results with hybrid RANS-LES modeling, the SA-DDES(IDDES) model implemented in MaPFlow follows the suggestions of [7], from hereon referred to as DDES.

3. Results

3.1. Numerical Predictions

In the present work the flow over the flatback airfoil at zero AoA is considered. In order to quantify the effect of grid resolution on the predictions, three grids with varying resolutions are generated, consisting of approximately 5, 10 and 25 million elements, respectively. The grids are hybrid, having a structured region close to the airfoil (boundary layer) and the rest of the domain is unstructured. In the spanwise direction, the mesh is extruded to one chord length and symmetry conditions are applied to the side boundaries. The spanwise resolution varies between 60 nodes on the coarser to 200 nodes on the finer grid. As the spanwise resolution increased, the structured boundary layer grid (i.e. the RANS region grid) remained unchanged in the chordwise and wall normal directions. On the other hand, the unstructured grid in the wake (i.e. up to 2.5 chord lengths downstream of the wing TE) is refined in all directions to maintain the cell aspect ratio close to unity. The same computational mesh is used for both URANS and DDES simulations to avoid grid related deviations. Details on the computational grid used can be found in Table 1.

Grid	Cells	Spanwise Spacing	Spanwise Nodes	$y+$
L3	$5 \cdot 10^6$	0.016	60	≈ 1
L2	$12 \cdot 10^6$	0.008	125	≈ 1
L1	$25 \cdot 10^6$	0.005	200	≈ 1

Table 1: Description of the computational grids used

Mean integrated loads for each computational mesh are first compared. The predicted lift (C_L) and drag (C_D) coefficient for each grid can be seen in Figure 2 and Figure 3 respectively. Evidently, the predicted loads when employing the L2 and L1 grids are in close agreement. The differences when using the coarser L3 grid are greater, especially for the URANS simulations. Regarding the comparison of URANS and DDES predictions, URANS simulations predict a higher mean C_L value whereas the results of C_D are in good agreement.

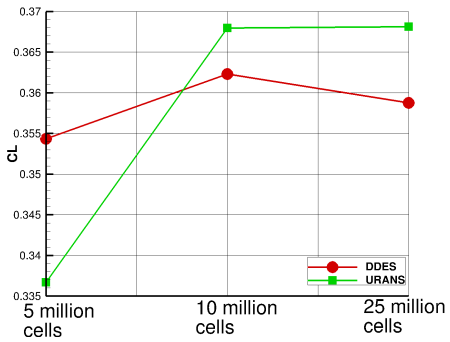

Figure 2: Lift Coefficient (C_L) as predicted for the various grids

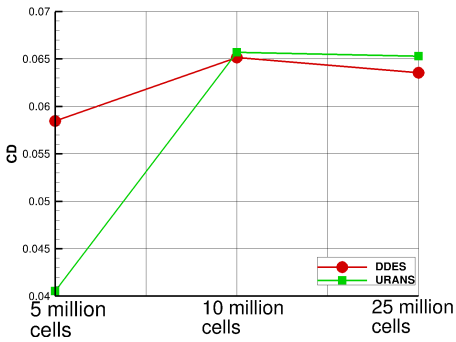

Figure 3: Drag Coefficient (C_D) as predicted for the various grids

Even though the initial comparison shows similar mean C_L, C_D values, the two methods are far apart when the unsteady characteristics are compared. Due to the thick trailing edge, the flow around the flatback airfoils is unsteady even at small AoAs. Indeed, vortices are continuously shed from the blunt trailing edge establishing a highly unsteady wake flow. The way URANS and DDES approaches predict the evolution of the wake has a direct impact on the predicted loads.

The C_L time histories from the URANS and DDES simulations are shown in Figure 4 and Figure 5, respectively. In URANS results, the C_L response to the vortex shedding frequency exhibits repeating patterns of increasing and after a while decaying amplitudes. This is more pronounced when the finer L2 and L1 grids are used, whereas it is not present when employing the coarser L3 grid. In the latter case, due to the increased numerical diffusion, the airfoil loads are primarily affected by the vorticity near the TE. The increased diffusion also confines the spanwise variation of vorticity.

On the contrary, DDES simulations do not exhibit the same characteristics. It is evident from Figure 5 that as the mesh resolution increases, the amplitude of the C_L signal also increases. However, the unphysical "beats" that the URANS simulations predict are not present in the DDES results.

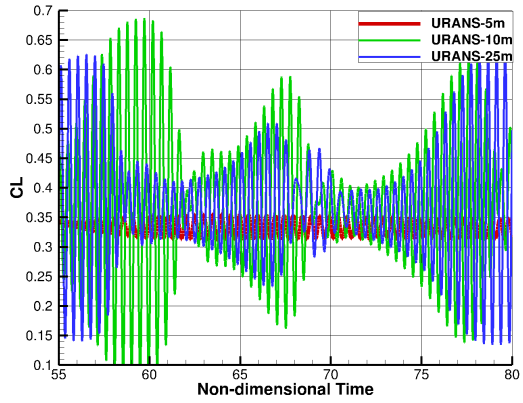

Figure 4: C_L time signal for the URANS simulations

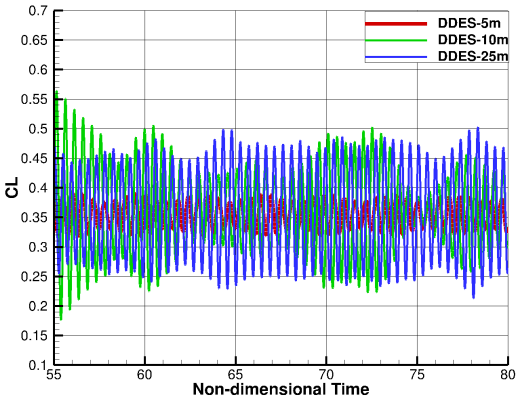

Figure 5: C_L time signal for the DDES simulations

The previous comments also apply to the C_D results. In Figure 6, where the C_D time histories from the URANS simulations are presented, it is clear that when the finer L2 and L1 grids are used the predictions exhibit large unphysical oscillations. These oscillations are not present in the DDES predictions shown in Figure 7. The URANS C_D signal also has two distinct frequencies, similar to what was observed in the URANS C_L signal (Figure 4). In the results using the coarser grid the amplitude of the C_D signal is very low due to the faster trailing edge vorticity diffusion.

Regarding the DDES drag predictions in Figure 7, all three grids yield approximately the same mean values. However, as the mesh resolution increases, the amplitude of the signal also increases, while additional frequencies are excited. Comparing the results from the medium grid (L2-10m cells) to those from the finer grid (L1-25m cells), the agreement is fair in terms of both C_L and C_D.

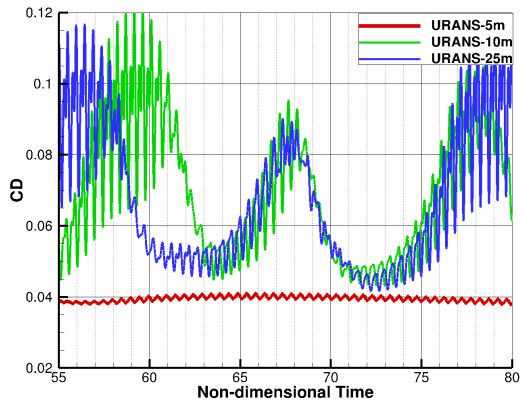

Figure 6: C_D time signal for the RANS simulations

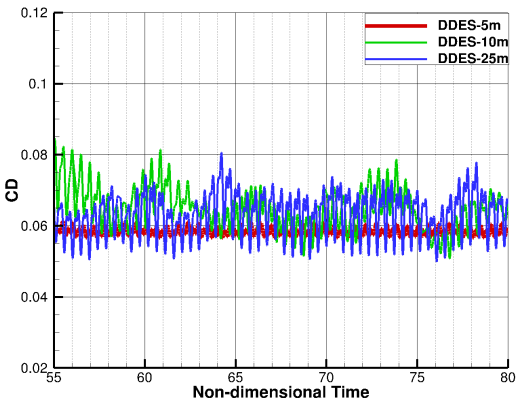

Figure 7: C_D time signal for the DES simulations

In order to have a better understanding of the unsteady flow characteristics, the spectral content of the C_L time histories is shown in Figure 8 and Figure 9. The power spectral density (PSD) is plotted against the Strouhal number ($St = \frac{fh_{TE}}{U_\infty}$). In the St number definition, f is the dominant shedding frequency, h_{TE} is the TE thickness and U_∞ is the free stream velocity. As Figure 9 suggests, when the computational grid is refined the main shedding frequency moves to the right in the DDES simulations. On the contrary, for the URANS simulations (Figure 8) the main shedding frequency remains unchanged even when using the coarse L3 grid. However, high energy at low frequencies is noted which is due to the repeating patterns (amplifications followed by decay response) shown in the CL time series of the URANS predictions (Figure 8).

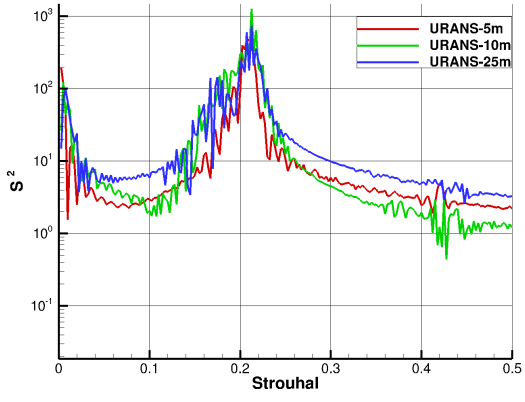

Figure 8: Power Spectral Density (PSD) of the C_L signal vs the Strouhal Number for the URANS simulations

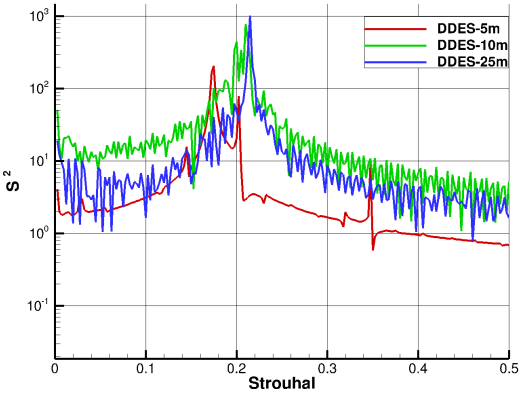

Figure 9: Power Spectral Density (PSD) of the C_L signal vs the Strouhal Number for the DDES simulations

Figure 10 and Figure 11 present a snapshot of the predicted vortical structures using the Q-criterion [15] for both URANS and DDES approaches. Figure 10 contains the results from the URANS simulation using the three successively refined meshes (from left to right). In the coarser grid (Figure 10a) the shed vorticity quickly decays, contrary to the finer grids where the

wake is preserved. Nevertheless, the wake predicted by the URANS simulations has coherent vortices in both the 10M (Figure 10b) and 25M meshes (Figure 10c). It is noticeable that when the 10M grid is employed, the wake exhibits stronger 3D effects that in the predictions using the finer grid. This is probably a grid induced artifact since it is not reproduced in the refined mesh. The fact that vorticity remains coherent in the URANS simulations can explain the excitation of the lower frequencies expressed as "beats" in the C_L and C_D time signals.

On the other hand in DDES simulations (Figure 11) wake structures are preserved even at the coarser grid which indicates that in DDES analysis the 3D character of the flow is revealed even with relatively coarse grids (Figure11a). Increasing the mesh resolution to 10M (Figure 11b) and 25M (Figure 11c) results to a better resolved vorticity patterns in the wake. Additionally in the medium and fine DDES simulations the generation of streamwise vorticity in the wake is evident. The main spanwise vortices give raise to multiple streamwise hairpin vortices.

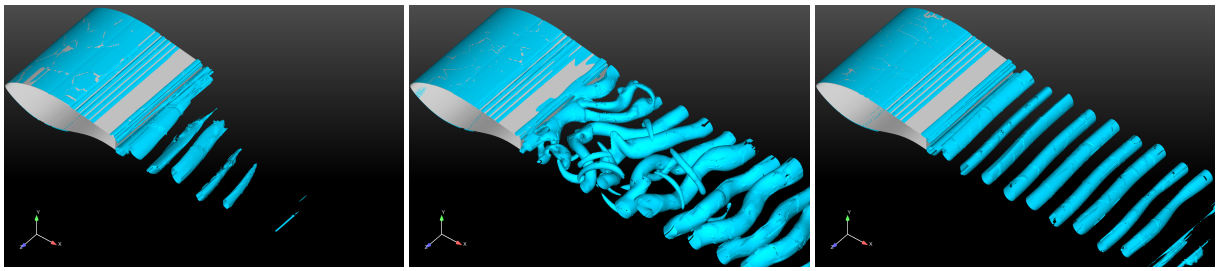

(a) RANS 5 million grid (b) RANS 10 million grid (c) RANS 25 million grid

Figure 10: RANS predictions – Isosurfaces of Q=1.5 coloured by streamwise vorticity. The 2D-like vortical structures are evident in the wake in the finer 10M and 25M meshes. On the coarser grid, vorticity decays rapidly.

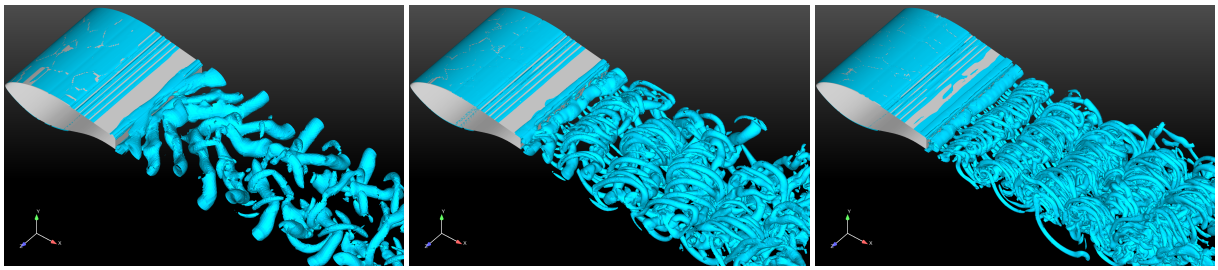

(a) DDES 5 million grid (b) DDES 10 million grid (c) DDES 25m miliion grid

Figure 11: DES predictions – Isosurfaces of Q=1.5 coloured by streamwise vorticity. The high three dimensionality of the flow can be seen even in the coarser 5 million grid. As the grid is refined more flow features are resolved

3.2. Comparison with Measurements

The comparisons between the experiments and the simulations in terms of lift coefficient (C_L), drag coefficient (C_D) and St number are given in Table 2. The dominant frequency is extracted from the velocity time series in the wake of the airfoil in the experiments, and from the C_L time signals in the simulations. As the grid is refined, both URANS and DDES simulations converge to $Str \approx 0.21$, which deviates by $\approx 10\%$ from the measured Str. Regarding the standard deviation of the C_L and C_D time signals, it is clear that the URANS results yield large load fluctuations, especially for C_D.

	C_L	C_D	C_L STD	C_D STD	St
Experiment	0.399	0.042	-	-	0.240
RANS(L3-5M cells)	0.347	0.052	0.0157	0.00075	0.207
DES (L3-5M cells)	0.353	0.059	0.0211	0.0011	0.200
RANS(L2-10M cells)	0.367	0.065	0.1123	0.0191	0.211
DES (L2-10M cells)	0.362	0.066	0.0802	0.0079	0.210
RANS(L1-25M cells)	0.366	0.060	0.0947	0.0194	0.211
DES(L1-25M cells)	0.361	0.064	0.0801	0.0060	0.214

Table 2: Lift and Drag Coefficient values,standard deviation (STD) and Strouhal number from the experiments and the different numerical cases

In Figures 12 and 13 time-averaged velocity fluctuation contours from experiments and simulations are shown. It is evident that the overall agreement with the experimental results is fair regardless of the turbulence modelling approach used. However, for both $\overline{u'u'}$ and $\overline{v'v'}$ the DDES simulations are in closer agreement with the PIV measurements. Regarding $\overline{u'u'}$ in Figure 12, both URANS and DDES underpredict the magnitude of the fluctuations when compared to the experimental data, although DDES simulations capture the asymmetry between the upper and lower side of the TE seen in the PIV measurements. Concerning $\overline{v'v'}$ in Figure 13, URANS results clearly underpredict the overall fluctuation magnitude, whereas DDES results are in very good agreement with the experimental data.

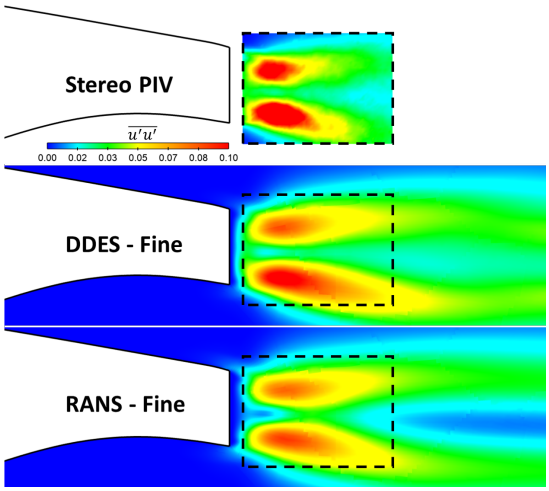

Figure 12: Normalized $\overline{u'u'}$ contours at the mid-plane normal to the wing span. The PIV plane limits are outlined by a dashed line on the numerical results. DDES simulation capture the assymetry evident in the measurements

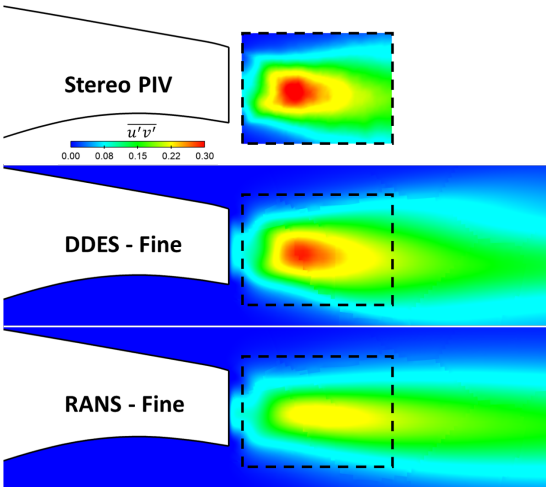

Figure 13: Normalized $\overline{v'v'}f$ contours at the mid-plane normal to the wing span. The PIV plane limits are outlined by a dashed line on the numerical results.DDES simulations are good agreement with the measurements.

The aforementioned comments also apply to the $\overline{u'v'}$ comparison as shown in Figure 14. It is evident that the URANS underpredict the time averaged velocity fluctuations as compared to the DDES simulations and the Stereo PIV measurements. It is noted here that a finer grid would probably make the comparison of the DDES simulations even better with the experimental data.

Finally, in Figure 15 time-averaged streamwise velocity contours are presented. Computations and measurements are in very good agreement regardless of the employed turbulence modeling

approach. DDES results are in better agreement with the PIV data, even though in this case the differences are marginal.

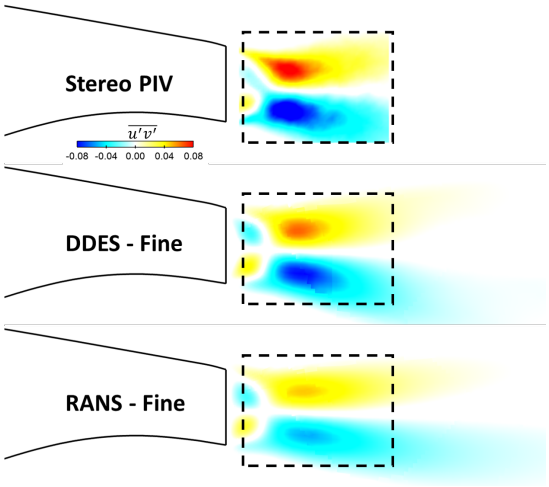

Figure 14: Normalized $\overline{u'v'}$ contours at the mid-plane normal to the wing span. The PIV plane limits are outlined by a dashed line on the numerical results.DDES simulations are good agreement with the measurements.

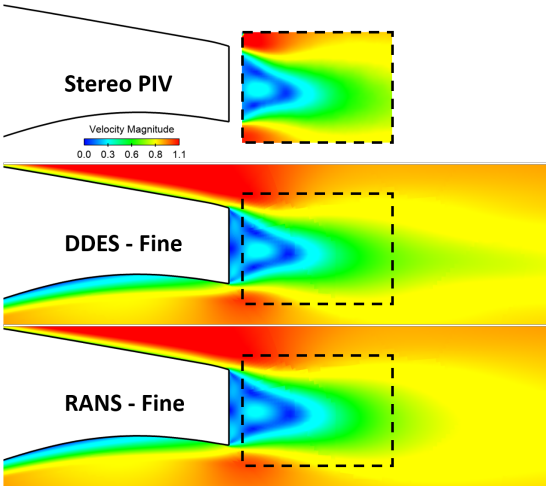

Figure 15: Time-averaged streamwise velocity contours at the mid-plane normal to the wing span. The PIV plane limits are outlined by a dashed line on the numerical results. DDES simulation capture the assymetry evident in the measurements

4. Conclusions

In the present work, the flow past a flat back airfoil has been investigated both computationally and experimentally. The focus was on the URANS-DDES turbulence modeling approach comparison in terms of prediction accuracy and overall wake behavior. The simulations utilized the SA-URANS and SA-DDES variants, using grids with increasing resolution. Identical meshes were used regardless of the turbulence modeling approach, to eliminate any grid-related discrepancies.

When comparing DDES and URANS predictions in terms of averaged spanwise loads, both models seem to accurately capture mean lift and drag values. However, a closer inspection of the C_L and C_D signals reveals that URANS results are qualitatively different from those using DDES. Interestingly, URANS simulations seem to deteriorate as the grid resolution increases.

The two methods agree fairly well when the coarser grid is employed. On the contrary, URANS results using finer meshes yield large load variations. These variations are not present in the experimental data and the DDES predictions and are attributed to the coherency of the shed vorticity in the URANS approach.

As the wake visualization suggests, when coarser grids are used in both URANS and DDES approaches, vorticity quickly decays and there is minimal spanwise variation. However, as mesh resolution increases, the results from URANS and DDES deviate. URANS predictions form coherent, 2D-like structures, which lead to large oscillations in the predicted loads. On the contrary, when DDES is employed the wake is highly three dimensional even when the coarser 5M grid is used. Results suggest that when dealing with separated flows, URANS predictions should be carefully examined, especially if very fine grids are utilized. The URANS approach has the tendency to enforce two-dimensionality, which can amplify the wake effect on the loads, leading to unphysical load fluctuations which are not present in experimental measurements.

Acknowledgments
Computational resources were provided by HPC Wales, which is gratefully acknowledged. M Manolesos would like to acknowledge the contribution of the Supergen Early Career Researcher Fund Award by the Supergen Offshore Renewable Energy Hub, EPSRC.

References
[1] J. P. Baker, E. A. Mayda, C. P. Van Dam, Experimental analysis of thick blunt trailing-edge wind turbine airfoils, Journal of Solar Energy Engineering, Transactions of the ASME 128 (4) (2006) 422–431. doi:10.1115/1.2346701.

[2] D. T. Griffith, P. W. Richards, The SNL100-03 Blade : Design Studies with Flatback Airfoils for the Sandia 100-meter Blade, Sandia National Laboratories Technical Report (September) (2014) 40.

[3] M. F. Barone, D. Berg, Aerodynamic and aeroacoustic properties of a flatback airfoil: An update, 47th AIAA Aerospace Sciences Meeting including the New Horizons Forum and Aerospace Exposition (2009). doi:10.2514/6.2009-271.

[4] G. Papadakis, M. Manolesos, The flow past a flatback airfoil with flow control devices: Benchmarking numerical simulations against wind tunnel data, preprint submitted to Wind Energy Science (February) (2020). doi:10.5194/wes-2020-36.

[5] C. Stone, S. N. Laboratories, C. E. Lynch, M. J. Smith, A Computational Study of the Aerodynamics and Aeroacoustics of a Flatback Airfoil Using Hybrid RANS-LES, 47th AIAA Aerospace Sciences Meeting and Exhibit (January) (2009) 1–24.

[6] P. R. Spalart, S. Deck, M. L. Shur, K. D. Squires, M. K. Strelets, A. Travin, A new version of detached-eddy simulation, resistant to ambiguous grid densities, Theoretical and Computational Fluid Dynamics 20 (3) (2006) 181–195. doi:10.1007/s00162-006-0015-0.

[7] M. L. Shur, P. R. Spalart, M. K. Strelets, A. K. Travin, A hybrid RANS-LES approach with delayed-DES and wall-modelled LES capabilities, International Journal of Heat and Fluid Flow 29 (6) (2008) 1638–1649. doi:10.1016/j.ijheatfluidflow.2008.07.001.
URL `http://dx.doi.org/10.1016/j.ijheatfluidflow.2008.07.001`

[8] M. Manolesos, S. G. Voutsinas, Experimental Study of Drag-Reduction Devices on a Flatback Airfoil, AIAA Journal (January) (2016) 1–15. doi:10.2514/1.J054901.
URL `http://arc.aiaa.org/doi/10.2514/1.J054901`

[9] G. Papadakis, S. G. Voutsinas, A strongly coupled Eulerian Lagrangian method verified in 2D external compressible flows, Computers and Fluids 195 (2019) 104325. doi:10.1016/j.compfluid.2019.104325.
URL `https://doi.org/10.1016/j.compfluid.2019.104325`

[10] G. Papadakis, S. G. Voutsinas, In view of accelerating CFD simulations through coupling with vortex particle approximations, Journal of Physics: Conference Series 524 (1) (2014) 012126. doi:10.1088/1742-6596/524/1/012126.
URL `http://stacks.iop.org/1742-6596/524/i=1/a=012126`

[11] K. Diakakis, G. Papadakis, S. G. Voutsinas, Assessment of transition modeling for high Reynolds flows, Aerospace Science and Technology 1 (2019) 1–13. doi:10.1016/j.ast.2018.12.031.
URL `https://doi.org/10.1016/j.ast.2018.12.031`

[12] P. L. Roe, Approximate Riemann solvers, parameter vectors, and difference schemes, Journal of Computational Physics 43 (2) (1981) 357–372. arXiv:arXiv:1011.1669v3, doi:10.1016/0021-9991(81)90128-5.

[13] S. Venkateswaran, J. Lindau, R. Kunz, C. Merkle, Preconditioning algorithms for the computation of multi-phase mixture flows, 39th Aerospace Sciences Meeting and Exhibit (January) (2001). doi:10.2514/6.2001-279.
URL `http://arc.aiaa.org/doi/10.2514/6.2001-279`

[14] P. R. Spalart, S. R. Allmaras, J. Reno, A One-Equatlon Turbulence Model for Aerodynamic Flows Boeing Commercial Airplane Group 30th Aerospace Sciences, AIAA paper 1992-0439 (1992). arXiv:arXiv:1011.1669v3, doi:10.2514/6.1992-439.

[15] J. C. R. Hunt, A. A. Wray, P. Moin, Eddies, streams, and convergence zones in turbulent flows, in: Studying Turbulence Using Numerical Simulation Databases, 2, Vol. 1, 1988, pp. 193–208.